Floquet scattering through a time-periodic potential

Wenjun Li and L. E. Reichl
Center for Studies in Statistical Mechanics and Complex Systems, The University of Texas at Austin, Austin, Texas 78712
(Received 11 June 1999)

Floquet scattering theory is developed to study electron transmission through a harmonically driven potential. The Floquet *S* matrix is constructed to calculate transmission probabilities as well as the Wigner delay times. Transmission resonances result from the interaction of electrons with the oscillating field by means of photon emission and absorption. Oscillator-induced quasibound states can accumulate electrons and give rise to electron interchannel transitions at resonances. Due to the oscillating potential, an ac Stark effect is observed. Floquet quasibound states appear as transmission poles in the complex energy plane. Lifetimes obtained from transmission poles are of the same order of magnitude as the corresponding Wigner delay times. [S0163-1829(99)02447-9]

I. INTRODUCTION

Transport in periodically driven mesoscopic systems is a subject of increasing importance because of a growing number of applications.[1–8] Photon-assisted tunneling has been observed in quantum resonant tunneling structures[9] such as $Al_xGa_{1-x}As/GaAs$ quantum dots,[10,11] quantum diodes,[12] and superlattices.[13] This phenomenon is expected to be used in designing high-speed switching devices and high-frequency (up to THz) radiation sources and detectors.[12,14] It is important to understand the mechanisms by which the time-varying external fields affect the transport properties of these devices. For strongly driven systems, a nonperturbative approach based on Floquet theory[15] can be used.[16,17] Using advanced computing techniques, it is now possible to take into account the inelastic contributions in which an incident wave is scattered into many photon sidebands (scattering channels).[18–20]

For systems where bound states exist in the absence of a driving field, even a weak driving field can cause propagating electrons at appropriate incident Fermi energies to undergo transitions between the spatially localized bound states and extended states in the continuum by means of photon emission and absorption. This process creates unique transmission resonances. It is also shown that under the oscillation, the energy of a bound state has a small yet finite ac Stark shift. When the strength of the driving field becomes great enough, quasibound states can be created which have no connection to bound states of the unperturbed system.

Quasibound states appear as poles of the transmission amplitude in the complex energy plane. The real part of the complex energy gives the energy level of that quasibound state, while the imaginary part gives its lifetime. An incident particle with energy equal to (or near) the energy of a quasibound state generally experiences significant delay in its transmission through the scattering region.

An electron wave with a single incident energy transmitting through an oscillating barrier has been studied by several authors.[1–3,6,7] In Ref. 3, a transfer matrix technique was used to calculate the transmission and reflection coefficients. Our Floquet scattering model consists of an infinite number of incoming and outgoing waves (channels) with the Floquet energy spacing of $\hbar\omega$ (energy of the photon) between two adjacent channels. The Floquet *S* matrix can be constructed and used to derive transmission probabilities as well as the Wigner delay times.

In Sec. II, we solve the time-periodic Schrödinger equation for our system using the Floquet theorem, and we use Floquet states to construct the Floquet *S* matrix. In Sec. III, we study the behavior of transmission probabilities for our one-dimensional (1D) modulated square potential. Transmission resonances due to the interaction between electrons and the oscillating field will be studied numerically for both weak and strong oscillation cases. In Sec. IV we examine the oscillator induced quasibound states and the ac Stark energy shift. In Sec. V we discuss quasibound-state-associated transmission poles in the complex energy plane. Lifetimes obtained from transmission poles are compared to the Wigner delay times in Sec. VI. Finally in Sec. VII we make some concluding remarks.

II. FLOQUET SCATTERING

The Floquet theorem allows us to convert the solution of a time-periodic Schrödinger equation into a time-independent eigenvalue problem. Let us consider electrons transmitting through a modulated potential which extends from $-L/2$ to $L/2$ (see Fig. 1). The potential is

$$V(x,t)=\begin{cases}0, & x<-L/2 \text{ and } x>L/2\\ V_0+V_1\cos(\omega t), & -L/2\leqslant x\leqslant L/2.\end{cases} \tag{1}$$

The Schrödinger equation can be written

$$i\hbar\frac{\partial}{\partial t}\psi(x,t)=-\frac{\hbar^2}{2\mu}\frac{\partial^2}{\partial x^2}\psi(x,t)+V(x,t)\psi(x,t), \tag{2}$$

where μ is the electron effective mass. For GaAs $\mu=0.067m_e$, where m_e is the mass of the free electron. We use a *single-electron* model so we neglect the electron-electron interactions, and we assume the temperature is low enough that electron-phonon interactions can be neglected as well.

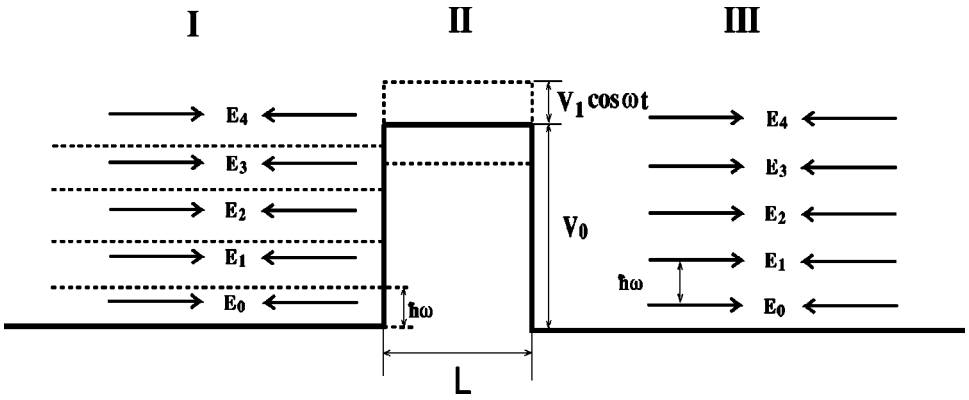

FIG. 1. Floquet scattering model. Incoming and outgoing waves (channels) have energy spacing of $\hbar\omega$ and are divided into Floquet zones according to $E_n = E_0 + n\hbar\omega$ $[n \in [0,\infty)]$. Floquet evanescent modes $[n \in (-\infty,-1]]$ also exist in the neighborhood of the oscillating barrier and do not propagate.

The Floquet theorem asserts that Eq. (2) has solutions of the form[15–17]

$$\psi_F(x,t) = e^{-iE_F t/\hbar}\phi(x,t), \tag{3}$$

where E_F is the Floquet eigenenergy and $\phi(x,t)$ is a periodic function: $\phi(x,t) = \phi(x,t+T)$, with period $T = 2\pi/\omega$. If we substitute Eq. (3) into Eq. (2), the Schrödinger equation takes the form

$$E_F\phi(x,t) = -\frac{\hbar^2}{2\mu}\frac{\partial^2}{\partial x^2}\phi(x,t) - i\hbar\frac{\partial}{\partial t}\phi(x,t) + V(x,t)\phi(x,t). \tag{4}$$

In order to solve the Schrödinger equation above, we will treat the three regions, $x < -L/2$, $-L/2 \leqslant x \leqslant L/2$, and $x > L/2$ (which we denote I, II, and III, respectively) separately and then match their wave functions at the boundaries.[1] We first consider region II.

A. Floquet solution inside the oscillating potential

Since $V(x,t)$ is space homogeneous inside region II, Eq. (4) is separable[6] and we can write $\phi(x,t) = g(x)f(t)$. This leads to the following equations for $g(x)$ and $f(t)$, respectively:

$$-\frac{\hbar^2}{2\mu}\frac{\partial^2}{\partial x^2}g(x) + V_0\, g(x) = E\, g(x), \tag{5}$$

$$i\hbar\frac{\partial}{\partial t}f(t) - V_1\cos(\omega t)f(t) = (E - E_F)f(t), \tag{6}$$

where E is a constant. Integrating Eq. (6) gives

$$f(t) = e^{-i(E-E_F)t/\hbar}\exp\left(-\frac{i}{\hbar}\int_0^t V_1\cos(\omega t')dt'\right) = e^{-i(E-E_F)t/\hbar}\sum_{n=-\infty}^{\infty} J_n\left(\frac{V_1}{\hbar\omega}\right)e^{-in\omega t}, \tag{7}$$

where we have taken $f(0) = 1$. Since $f(t) = f(t+T)$, Eq. (7) requires that $E = E_F + m\hbar\omega$, where m is an integer.

The equation for $g(x)$ has a solution

$$g(x) = \sum_{m=-\infty}^{\infty}(a_m e^{iq_m x} + b_m e^{-iq_m x}), \tag{8}$$

where a_m and b_m are constant coefficients and

$$\frac{\hbar^2 q_m^2}{2\mu} = E_F + m\hbar\omega - V_0. \tag{9}$$

By combining the solutions for $f(t)$ and $g(x)$, we obtain the following expression for the Floquet state, $\psi^{\mathrm{II}}(x,t)$, inside the oscillating region:

$$\psi^{\mathrm{II}}(x,t) = e^{-iE_F t/\hbar}\sum_{n=-\infty}^{\infty}\sum_{m=-\infty}^{\infty}(a_m e^{iq_m x} + b_m e^{-iq_m x})J_{n-m}\left(\frac{V_1}{\hbar\omega}\right)e^{-in\omega t}. \tag{10}$$

$\psi^{\mathrm{II}}(x,t)$ resembles the Tien-Gordon wave functions in microwave-driven superconductor films.[21] The Floquet energy E_F and coefficients a_m and b_m will be determined by the boundary conditions.

B. Floquet solution outside the oscillating potential

Since electrons incident to the oscillating region will be scattered inelastically into Floquet sidebands, the wave function outside the barrier must consist of many Floquet sidebands in order to match the boundary conditions at $x = \pm L/2$.

Let us assume that the incoming and outgoing particle waves on both sides of the scatterer are superpositions of an infinite number of sidebands with energy spacing of $\hbar\omega$, as shown in Fig. 1. The potential in region I and III is zero. The wave function in these free particle regions can be written:

$$\psi^{\mathrm{I}}(x,t) = \sum_{n=-\infty}^{\infty}(A_n^i e^{ik_n x - iE_n t/\hbar} + A_n^o e^{-ik_n x - iE_n t/\hbar}), \tag{11}$$

$$\psi^{\mathrm{III}}(x,t) = \sum_{n=-\infty}^{\infty}(B_n^i e^{-ik_n x - iE_n t/\hbar} + B_n^o e^{ik_n x - iE_n t/\hbar}), \tag{12}$$

where A_n^i and B_n^i are the probability amplitudes of the incoming waves from the left and right, respectively, while A_n^o and B_n^o are those of the outgoing waves. The incoming waves are divided into different zones with index n: $E_n = E_0 + n\hbar\omega$, where $E_0 \in [0,\hbar\omega)$ is the Floquet energy of the *propagating mode* with the lowest energy.

It is important to note that Eqs. (11) and (12) also involve modes with energies below E_0 (in the sum n can be negative). When $E_n<0$, $k_n=\sqrt{2\mu E_n/\hbar^2}$ is imaginary. Such a mode will not propagate and is called an evanescent mode.[19] The current density for an evanescent mode is zero.

C. The Floquet S matrix

The Floquet eigenenergy E_F in Eq. (3) can be determined up to an arbitrary integer multiplied by $\hbar\omega$, since according to Eq. (10) shifting E_F by $n\hbar\omega$ does not change the wave function $\psi^{\rm II}(x,t)$. For convenience, we choose E_F within the lowest zone, $E_F=E_0$.

The wave function, $\psi(x,t)$, and its first derivative must be continuous at the boundaries $x=\pm L/2$. At $x=-L/2$ this leads to

$$A_n^i e^{-ik_n L/2}+A_n^o e^{ik_n L/2}=\sum_{m=-\infty}^{\infty}(a_m e^{-iq_m L/2}+b_m e^{iq_m L/2})J_{n-m}\left(\frac{V_1}{\hbar\omega}\right) \tag{13}$$

and

$$ik_n A_n^i e^{-ik_n L/2}-ik_n A_n^o e^{ik_n L/2}=\sum_{m=-\infty}^{\infty}(iq_m a_m e^{-iq_m L/2}-iq_m b_m e^{iq_m L/2})J_{n-m}\left(\frac{V_1}{\hbar\omega}\right). \tag{14}$$

Similarly, at $x=L/2$ we have

$$B_n^i e^{-ik_n L/2}+B_n^o e^{ik_n L/2}=\sum_{m=-\infty}^{\infty}(a_m e^{iq_m L/2}+b_m e^{-iq_m L/2})J_{n-m}\left(\frac{V_1}{\hbar\omega}\right), \tag{15}$$

and

$$-ik_n B_n^i e^{-ik_n L/2}+ik_n B_n^o e^{ik_n L/2}=\sum_{m=-\infty}^{\infty}(iq_m a_m e^{iq_m L/2}-iq_m b_m e^{-iq_m L/2})J_{n-m}\left(\frac{V_1}{\hbar\omega}\right). \tag{16}$$

Eliminating A_n^o from Eqs. (13) and (14) yields

$$\sum_{m=-\infty}^{\infty}[(k_n+q_m)e^{-iq_m L/2}a_m+(k_n-q_m)\times e^{iq_m L/2}b_m]J_{n-m}\left(\frac{V_1}{\hbar\omega}\right)=2A_n^i k_n e^{-ik_n L/2}. \tag{17}$$

Eliminating B_n^o from Eqs. (15) and (16) gives

$$\sum_{m=-\infty}^{\infty}[(k_n-q_m)e^{iq_m L/2}a_m+(k_n+q_m)\times e^{-iq_m L/2}b_m]J_{n-m}\left(\frac{V_1}{\hbar\omega}\right)=2B_n^i k_n e^{-ik_n L/2}. \tag{18}$$

If we combine Eqs. (17) and (18), we obtain the following infinite matrix equation:

$$\sum_{m=-\infty}^{\infty}[(k_n+q_m)e^{-iq_m L/2}\pm(k_n-q_m)e^{iq_m L/2}]J_{n-m}\left(\frac{V_1}{\hbar\omega}\right)C_m^{\pm}=2(A_n^i\pm B_n^i)k_n e^{-ik_n L/2}, \tag{19}$$

where $C_m^{\pm}=a_m\pm b_m$.

If the incoming amplitudes A_n^i and B_n^i are given, then Eq. (19) determines the coefficients $C_m^{\pm}$. All other quantities of interest can be obtained from these coefficients. [In practice, we must use a truncated version of Eq. (19).] The coefficients a_m and b_m are given by $a_m=(C_m^+ + C_m^-)/2$ and $b_m=(C_m^+ - C_m^-)/2$. The probability amplitudes of the outgoing waves are given by

$$A_n^o=\sum_{m=-\infty}^{\infty}(a_m e^{-iq_m L/2}+b_m e^{iq_m L/2})J_{n-m}\left(\frac{V_1}{\hbar\omega}\right)e^{-ik_n L/2}-A_n^i e^{-ik_n L} \tag{20}$$

and

$$B_n^o=\sum_{m=-\infty}^{\infty}(a_m e^{iq_m L/2}+b_m e^{-iq_m L/2})J_{n-m}\left(\frac{V_1}{\hbar\omega}\right)e^{-ik_n L/2}-B_n^i e^{-ik_n L}. \tag{21}$$

Equations (20) and (21) can be expressed in matrix form (see the Appendix):

$$\begin{pmatrix}\mathbf{A}^o\\ \mathbf{B}^o\end{pmatrix}=\mathcal{S}\begin{pmatrix}\mathbf{A}^i\\ \mathbf{B}^i\end{pmatrix}, \tag{22}$$

where $\mathbf{A}^i,\mathbf{B}^i$ and $\mathbf{A}^o,\mathbf{B}^o$ are the incoming and outgoing (including the associated evanescent Floquet sidebands) amplitude vectors, respectively. The matrix $\mathcal{S}$ consists of all the probability amplitudes which connect the coefficients $\mathbf{A}^i,\mathbf{B}^i$ to coefficients $\mathbf{A}^o,\mathbf{B}^o$.

If we keep only the propagating modes, then we obtain the scattering S matrix, $\overline{\mathbf{S}}$, which satisfies the equation

$$\begin{pmatrix}\overline{\mathbf{A}}^o\\ \overline{\mathbf{B}}^o\end{pmatrix}=\overline{\mathbf{S}}\begin{pmatrix}\overline{\mathbf{A}}^i\\ \overline{\mathbf{B}}^i\end{pmatrix}. \tag{23}$$

This unitary S matrix is determined by the transmission and reflection amplitudes for the propagating modes,

$$\overline{\mathbf{S}}=\begin{pmatrix}\overline{\mathbf{R}} & \overline{\mathbf{T}}'\\ \overline{\mathbf{T}} & \overline{\mathbf{R}}'\end{pmatrix}=\begin{pmatrix} r_{00} & r_{01} & \cdot\cdot & t'_{00} & t'_{01} & \cdot\cdot\\ r_{10} & r_{11} & \cdot\cdot & t'_{10} & t'_{11} & \cdot\cdot\\ \cdot & \cdot & & \cdot & \cdot & \\ \cdot & \cdot & & \cdot & \cdot & \\ t_{00} & t_{01} & \cdot\cdot & r'_{00} & r'_{01} & \cdot\cdot\\ t_{10} & t_{11} & \cdot\cdot & r'_{10} & r'_{11} & \cdot\cdot\\ \cdot & \cdot & & \cdot & \cdot & \\ \cdot & \cdot & & \cdot & \cdot & \end{pmatrix}, \tag{24}$$

where r_{nm} and t_{nm} are the reflection and transmission amplitudes, respectively, for modes incident from the left; r'_{nm} and t'_{nm} are similar quantities for modes incident from the right. Here $n,m\in[0,\infty)$ since matrix $\overline{\mathbf{S}}$ contains only the reflection and transmission amplitudes of the propagating modes. Elements such as $t_{-1,0}$, $r_{-1,0}$ in matrix $\mathcal{S}$ correspond to probability amplitudes describing an electron with incident energy E_0 being scattered into the evanescent mode E_{-1} (with energy $\hbar\omega$ below E_0).

From the scattering S matrix we can obtain the total transmission coefficient:

$$T=\sum_{n=0}^{\infty}\sum_{m=0}^{\infty}\frac{k_n}{k_m}|t_{nm}|^2. \tag{25}$$

Other scattering quantities, such as eigenphases and scattering delay times can also be derived from the S matrix. We will discuss this in later sections.

If we consider a single electron wave incident from one direction (say the left) with a fixed Fermi energy E_0 and wave vector k_0, there is only one element, A_0^i, that is nonzero in the incoming amplitude vector, and the transmission coefficient T calculated from Eq. (25) involves only t_{n0} ($m=0$ and n varies over all the transmitted propagating sidebands). If the incident energy belongs to a higher energy zone m $[m\hbar\omega\leqslant E_{in}<(m+1)\hbar\omega]$, we use t_{nm} in the corresponding column in the S matrix. According to the Landauer-Büttiker formula,[22] the total conductance of our oscillating device is

$$G=\frac{2e^2}{h}T. \tag{26}$$

The conductance G can be measured in experiments.

III. TRANSMISSION RESONANCES

In this section, we study numerically the scattering of a single incident wave through an oscillating square potential and we calculate the transmission coefficients.

The interaction of electrons with the oscillating potential leads to photon-mediated transmission resonances. In Fig. 2 we plot the transmission coefficient T as a function of the incident electron energy for $V_0=-20$ meV, $V_1=5$ meV, $L=10$ Å, and $\hbar\omega=1$ meV. Besides the incident channel $E=E_0$, five Floquet sidebands both above and below E_0 are taken into account, $E_n=E_0+n\hbar\omega$ with $n=0,\pm1,\ldots,\pm N$ and $N=5$. The minimum number of sidebands that need to be included is determined by the strength of the oscillation.

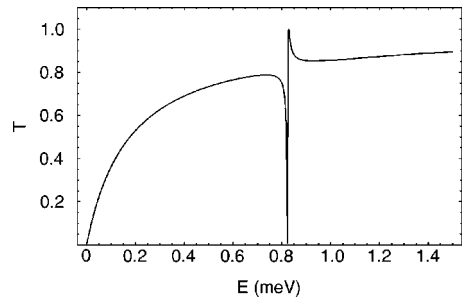

FIG. 2. The transmission coefficient T as a function of incident energy for system parameters $\hbar\omega=1$ meV, $V_0=-20$ meV, $V_1=5$ meV, $L=10$ Å. Sidebands $n=0,\pm1,\ldots,\pm5$ are taken into account so $T=\Sigma_{n=0}^{5}|t_{0n}|^2$. A resonance occurs at $E\approx0.826$ meV.

We should have $N>V_1/\hbar\omega$.[20] The transmission pattern has an asymmetric ''Fano'' resonance[23] at $E\approx0.826$ meV, where a sharp dip is followed by a peak. In this case, the deep quantum well ($V_0=-20$ meV, $L=10$ Å) ensures that there exists a bound state (when $V_1=0$, this bound state has energy $E_B=-0.17382$ meV). At the energy level where the resonance occurs, electrons in the incident channel ($E=\hbar\omega-|E_B|\approx0.826$ meV) can emit photons and drop to the ''bound'' state. Similarly, electrons in the ''bound'' state can absorb photons and jump to the incident channel (also other Floquet channels). A transmission resonance takes place when the energy difference between the incident channel and the bound state is equal to the energy of one or more photons. Figure 3 shows the transmission amplitudes t_{00} and $t_{-1,0}$ (the absolute values squared) as a function of incident energy. (Hereafter we use t_{n0} to denote the transmission amplitude from the incident channel to the nth Floquet sideband.) We can see clearly the accumulation of electrons in the bound state (which is now also the Floquet sideband E_{-1}). Since electrons in the evanescent mode will not propa-

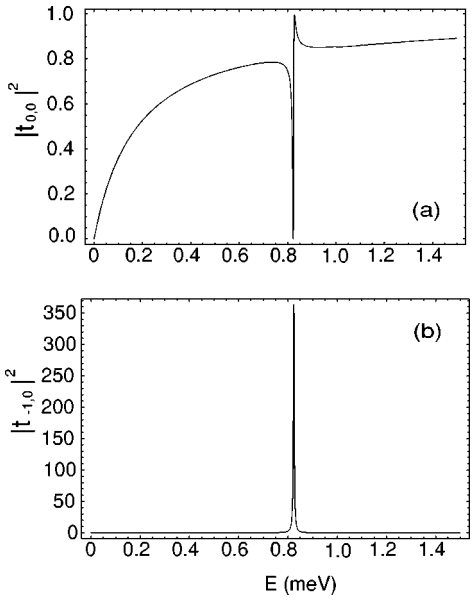

FIG. 3. Comparison of the transmission amplitudes of sidebands. (a) $|t_{0,0}|^2$ and (b) $|t_{-1,0}|^2$. (b) shows the accumulation of electrons in the bound state. The system parameters are $\hbar\omega=1$ meV, $V_0=-20$ meV, $V_1=5$ meV, $L=10$ Å.

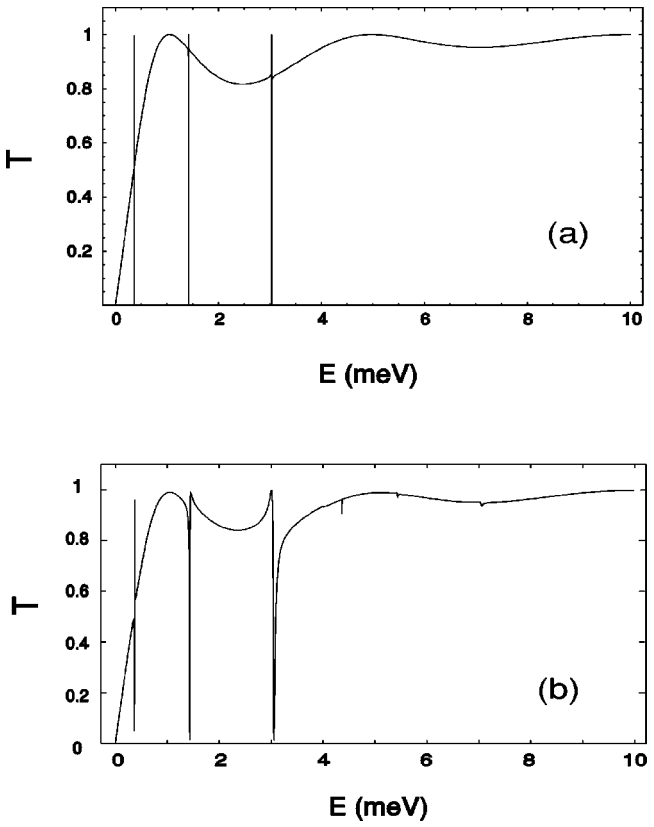

FIG. 4. The transmission coefficient T for system parameters $\hbar\omega=4$ meV, $V_0=-4$ meV, $V_1=0.1$ meV (a) and 1.0 meV (b), $L=1000$ Å. Transmission resonances show the existence of three static bound states. The resonance energy shifts below $\hbar\omega=4.0$ meV match well the bound state energies. Sidebands $n=0, \pm 1, \ldots, \pm 40$ are taken into account so $T=\Sigma_{n=0}^{40}|t_{0n}|^2$. (b) shows the higher-order resonances, which is almost invisible in (a) since there the oscillation is so weak.

gate, they make no contribution to the transmission coefficient.

When several bound states exist as is the case for Fig. 4, we see more than one transmission resonance. For this weak oscillator case we take $V_0=-4$ meV, $V_1=0.1$ meV and 1.0 meV, $L=1000$ Å, and $\hbar\omega=4$ meV. The three resonances below $E=\hbar\omega=4.0$ meV in Fig. 4(a) ($E=3.0375, 1.4243$, and 0.3637 meV) are due to the three bound states of the quantum well. By calculating the binding energies of those three bound states ($E_{B1}=-0.9625$ meV, $E_{B2}=-2.5758$ meV, $E_{B3}=-3.6363$ meV), we find that they are in good agreement with the resonance energy shifts below 4.0 meV. Figure 4(b) shows an increase in the oscillation strength, and we find that the resonances broaden and higher-order resonances start to appear.

As the strength of the oscillator, V_1, becomes greater, new quasibound states can be created due to the oscillating field. An example is shown in Fig. 5, where $V_0=0$ meV, $V_1=50$ meV, $L=20$ Å, and $\hbar\omega=2$ meV. In this case, the unperturbed system has no bound states. However, we see a resonance dip at $E=1.2$ meV, which lies 0.8 meV below $E=\hbar\omega=2.0$ meV. This energy shift is very similar to previous cases and suggests the existence of a quasibound state, as will be discussed below.

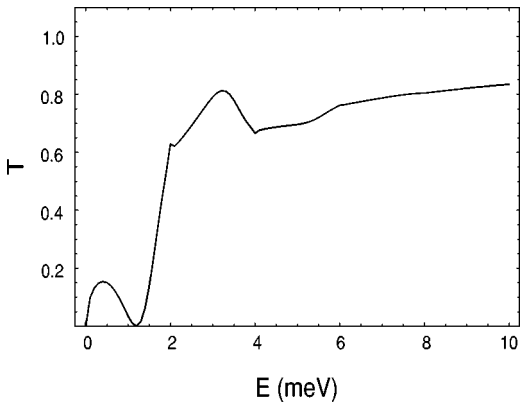

FIG. 5. The transmission coefficient T for system parameters $\hbar\omega=2$ meV, $V_0=0$ meV, $V_1=50$ meV, $L=20$ Å. The transmission zero below $E=\hbar\omega$ implies the existence of an oscillator induced quasibound state. Sidebands $n=0, \pm 1, \ldots, \pm 5$ are taken into account so $T=\Sigma_{n=0}^{5}|t_{0n}|^2$.

IV. OSCILLATOR-INDUCED QUASIBOUND STATES AND ac STARK SHIFT

The transmission zero in Fig. 5 implies the existence of a long-lived localized state (quasibound state) inside the oscillating potential which can accumulate electrons and produce a transmission resonance. To show the existence of such states and find their energies, we follow the same steps we used earlier in deriving the scattering S matrix, except that now we set all the A_n^i's and B_n^i's to zero. The existence of a system bound state or quasibound state ensures that even if there is no incident wave, we can still find a nonvanishing solution for the wave function.

Let us rewrite Eq. (19) as

$$\sum_{m=-\infty}^{\infty}[(k_n+q_m)e^{-iq_mL/2}\pm(k_n-q_m)e^{iq_mL/2}]J_{n-m}\left(\frac{V_1}{\hbar\omega}\right)C_m^{\pm}$$

$$\equiv \mathbf{M}_s^{\pm}\cdot\mathbf{C}^{\pm}=\mathbf{0}, \tag{27}$$

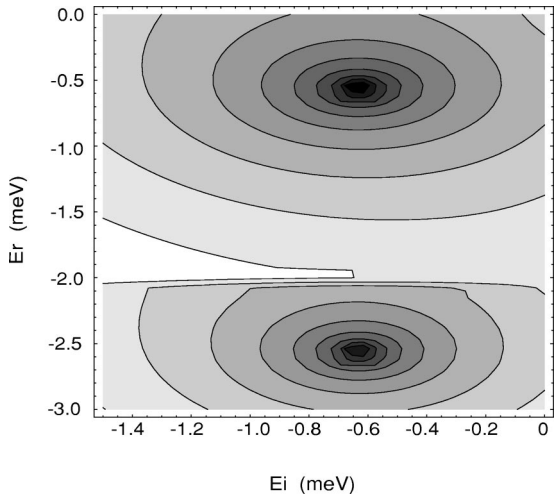

FIG. 6. The determinant of the state matrix in the complex energy plane for $\hbar\omega=2$ meV, $V_0=0$ meV, $V_1=50$ meV, $L=20$ Å. Black dots [corresponding to $\det(\mathbf{M}_s^{+})=0$] locate the complex energies (E_r denotes the real part, while E_i denotes the imaginary part) of Floquet quasibound states. Sidebands $n=0, \pm 1, \pm 2, \ldots, \pm 40$ are taken into account.

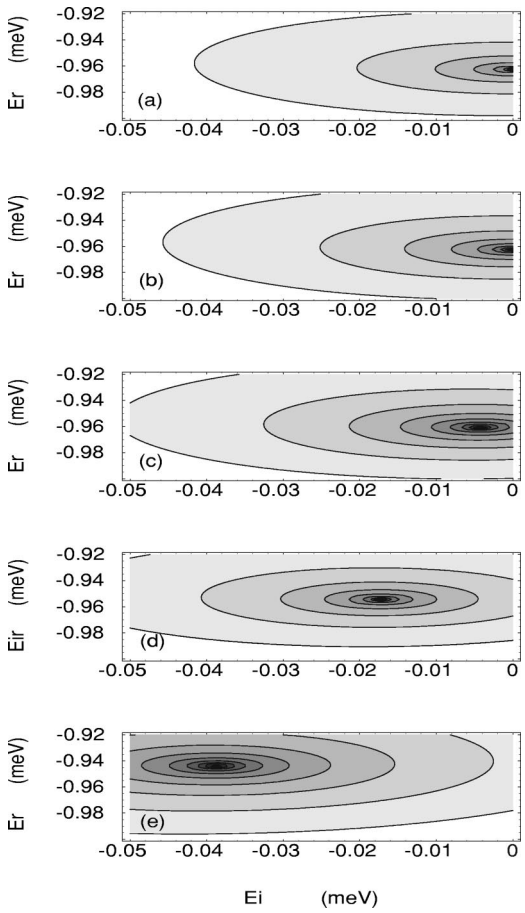

FIG. 7. The dark regions locate solutions of $\det(\mathbf{M}_s^+)=0$ for $\hbar\omega=4$ meV, $V_0=-4$ meV, $L=1000$ Å and (a) $V_1=0.0$ meV, (b) $V_1=0.1$ meV, (c) $V_1=0.5$ meV, (d) $V_1=1.0$ meV, and (e) $V_1=1.5$ meV. By increasing oscillating field strength, a static bound state becomes a quasibound state with a decreasing lifetime. Sidebands $n=0,\pm1,\ldots,\pm5$ are taken into account.

where $\mathbf{C}^{\pm}$ is an infinite dimensional vector and $\mathbf{M}_s^{\pm}$ is an infinite dimensional square matrix, which will be referred to as the state matrix. To get nonvanishing $\mathbf{C}^{\pm}$, the matrix $\mathbf{M}_s^{\pm}$ must be singular and we must have

$$\det(\mathbf{M}_s^{\pm})=0. \tag{28}$$

By solving Eq. (28), we can obtain the energy spectrum of Floquet quasibound states for the oscillating system.

Equation (28) has solutions for complex values of the energy, which indicates that the states associated with these solutions are not real bound states, but rather they are quasibound states with finite lifetimes. In addition, since shifting the energy in the infinite matrix $\mathbf{M}_s^{\pm}$ by any $n\hbar\omega$ essentially does not change its analytic properties, it follows that if E is a solution of Eq. (28), then $E+n\hbar\omega$ must be a solution also. It turns out that Eq. (28) always gives a set of quasibound states with the Floquet energy spacing of $\hbar\omega$.

As an example, the behavior of $\det(\mathbf{M}_s^+)$ as a function of complex energy is shown in Fig. 6. Hereafter we will use E_r and E_i to denote the real and imaginary part of the complex energy. This figure shows the quasibound state associated with the transmission resonance in Fig. 5 at $E=1.2$ meV. A very dark region $[\det(\mathbf{M}_s^+)=0]$ locates the complex energy

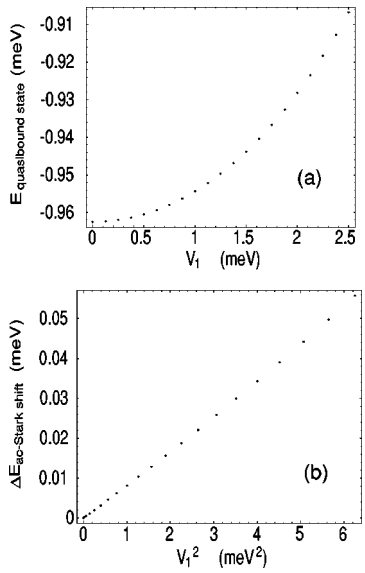

FIG. 8. ac Stark energy shift. Parameters are the same as Fig. 7 except 20 V_1's (oscillation strength) are calculated and sidebands $n=0,\pm1,\ldots,\pm5$ are used. (a) shows the change of E_r when V_1 increases and (b) illustrates that the magnitude of the ac Stark shift is approximately proportional to V_1^2 when V_1 is small.

of a quasibound state. The distance between two adjacent dark points is equal to the Floquet energy spacing of $\hbar\omega$. These Floquet quasibound states play a role similar to the static bound states in Figs. 2 and 4. This explains the energy shift of the resonance below $E=\hbar\omega$ in Fig. 5.

In the cases of Figs. 2 and 4, the system bound states have already been driven into the complex energy plane by the oscillating field. The ''bound states'' we referred to there are very close to the real energy axis because the oscillations are so weak. If we look at the complex energy plane, as shown in Fig. 7, we see clearly that as the oscillation strength increases, the original bound state moves away from the real energy axis. This picture expands the remarks made in Ref. 7, where all the discussion was restricted to the real energy axis. In fact, when an oscillating field is present, there are no longer any true bound states. Furthermore, the real part of the energy of the quasibound state changes slightly from its original bound state energy when it goes into the complex energy plane. Quantitative analysis shows that for weak oscillation, this ac Stark shift is approximately proportional to the square of the oscillation strength (V_1^2), as shown in Fig. 8.

V. TRANSMISSION POLES IN THE COMPLEX ENERGY PLANE

Another way to find quasibound states is to locate the poles of transmission probabilities, $|t_{nm}|^2$, in the complex energy plane. As is well known, for scattering through a static barrier $(V_1=0)$, there is a transmission pole in the complex energy plane associated with a transmission resonance $(T=1)$, which indicates the existence of a quasibound state. The real part of the quasibound state energy approximately locates the resonance energy, while the imaginary part is inversely proportional to the lifetime.[24] At the transmission resonance, an electron will stay in the neighborhood

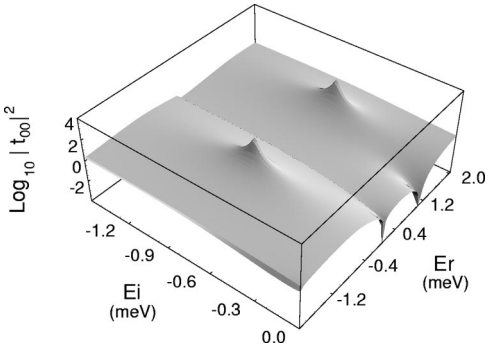

FIG. 9. Transmission poles in the complex energy plane for $\hbar\omega=2$ meV, $V_0=0$ meV, $V_1=50$ meV, $L=20$ Å.

of the scatterer for a relatively long time because the particle wave undergoes multiple reflections in the region $-L/2\leqslant x \leqslant L/2$. Once the incident wave turns off, it will decay very quickly with the rate governed by its lifetime.

For the case of Floquet scattering, the Floquet quasibound states also give rise to transmission resonances. In the complex energy plane, we also see poles of the S matrix associated with the quasibound states. For example, the transmission zero (due to resonance) at $E\approx 1.2$ meV in Fig. 5 is associated with a transmission pole in the complex energy plane which is shown in Fig. 9. In Fig. 9, we show the transmission probability $|t_{00}|^2$. Other S-matrix elements will also have poles. The distance between the two poles in Fig. 9 is equal to $\hbar\omega$. As mentioned earlier, each Floquet quasibound state is actually a member of a set of quasibound states. The transmission poles corresponding to these quasibound states line up in the complex energy plane with spacing along the real axis of $\hbar\omega$ between adjacent poles (when they are from the same set), they have the same distance from the real energy axis.

The transmission poles due to static quasibound states can exist in the complex energy plane alongside those induced by the field. Figure 10 [same parameters as in Fig. 4(a)] shows the coexistence of two types of transmission poles. If we compare Fig. 4(a) and Fig. 10, we see that in Fig. 10 the three poles near the real energy axis correspond to the three Floquet resonances (they belong to different Floquet quasibound state sets), while the pole farther away from the real energy axis corresponds to a resonant quasibound state due to the static quantum well [in Fig. 4(a) the resonance is located at $E=1.05$ meV]. A small part of one more pole with a higher energy (which corresponds to another static resonant quasibound state) is also visible at the far corner [$E=4.98$ meV in Fig. 4(a)].

The distance from the real energy axis of each pole determines the lifetime of the quasibound state:

$$\tau_L=\frac{\hbar}{\gamma}, \tag{29}$$

where $\gamma=2E_i$ and E_i is the imaginary part of the transmission pole energy. We will compare this lifetime with the Wigner delay time derived from the S matrix in the following section.

VI. WIGNER DELAY TIMES

The Wigner delay time gives the time delay of the scattered electron due to its interaction with the scattering field (here the oscillating potential). At the resonance, the incident wave excites a quasibound state in the neighborhood of the scatterer and the electron is delayed. As a result, the Wigner delay time will show a peak. To obtain the Wigner delay time, we use the scattering S matrix, $\overline{\mathbf{S}}$, derived in Sec. II. Its eigenvalues lie on the unit circle and can be written in the

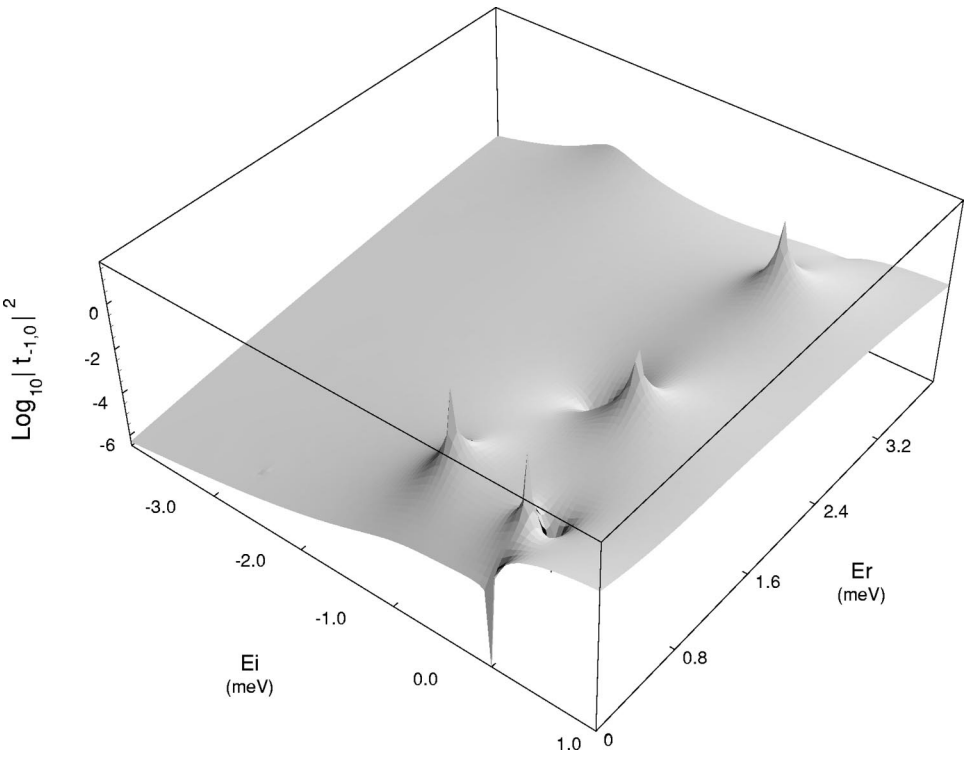

FIG. 10. Static and dynamic quasibound state poles for $\hbar\omega=4$ meV, $V_0=-4$ meV, $V_1=0.1$ meV, $L=1000$ Å. The three poles close to the real energy axis are due to the oscillating field. The remaining pole is due to the static quasibound state. A small part of another pole due to a static quasibound state is also visible at the far corner.

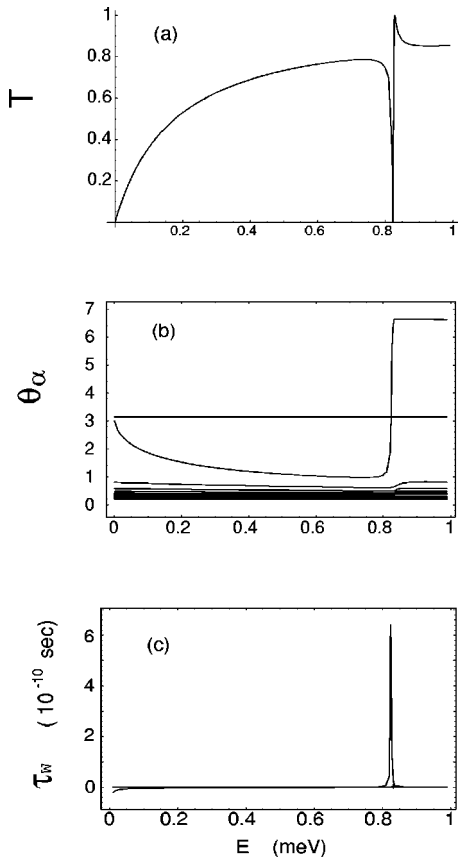

FIG. 11. (a) Transmission coefficient; (b) eigenphases of the S matrix; (c) Wigner delay times for $\hbar\omega=1$ meV, $V_0=-20$ meV, $V_1=5$ meV, $L=10$ Å. Floquet sidebands include $n=0,\pm1,\pm2,\ldots,\pm10$.

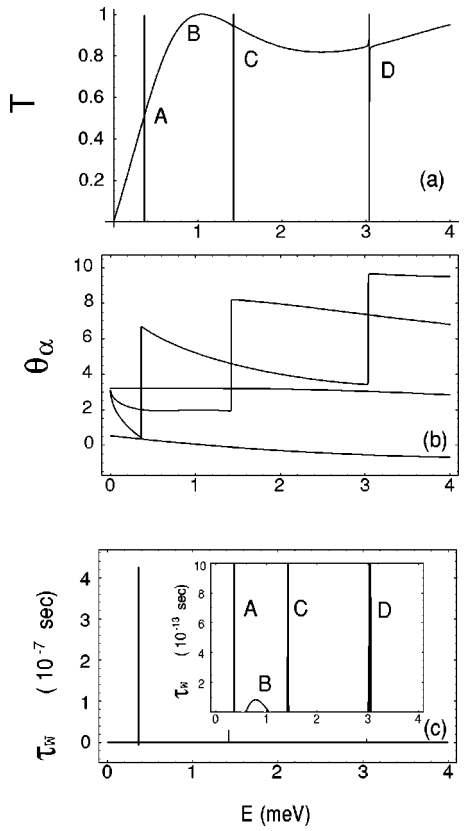

FIG. 12. (a) Transmission coefficient; (b) eigenphases; (c) Wigner delay times for $\hbar\omega=4$ meV, $V_0=-4$ meV, $V_1=0.1$ meV, $L=1000$ Å. Floquet sidebands $n=0,\pm1$ are included so the S matrix has four eigenvalues. Besides three dynamic resonances A, C, and D, the inset in the bottom figure also shows the Wigner delay time peak due to the static resonance B.

form $e^{i\theta_\alpha}$, where $e^{i\theta_\alpha}$ is the αth eigenvalue of the scattering S matrix (θ_α is the αth eigenphase). When there are $N+1$ propagating modes ($E_n=E_0+n\hbar\omega$ and $n=0,1,\ldots,N$), α runs from 1 to $2(N+1)$ since the S matrix is a $[2(N+1)]\times[2(N+1)]$ square matrix. The Wigner delay time

$$\tau_w^\alpha=\hbar\frac{d\theta_\alpha}{dE}$$

is the slope of the eigenphase as a function of the incident energy. In Fig. 11 (with the same parameters as in Fig. 2), we show the transmission coefficient, eigenphases, and Wigner delay times, respectively. We see that at the resonance, there is a Wigner delay time peak which indicates the electrons being delayed in the scattering region. From Fig. 12, we see that associated with each resonance (including the three Floquet dynamic resonances, which are marked as A, C, and D, respectively, as well as one static resonance marked as B), there is a Wigner delay time peak.

Table I compares the Wigner delay times and the corresponding lifetimes obtained from the transmission poles in the complex energy plane. τ_L is the lifetime defined in the previous section while τ_W is the maximum value of the corresponding Wigner delay time peak. They are of the same order of magnitude for all the cases considered. A similar comparison was done for an electron waveguide with no oscillating field by Na and Reichl and they obtained similar results.[25]

VII. CONCLUSIONS

In this paper we have considered 1D scattering through an oscillating square potential and developed the Floquet scattering theory for this model. The Floquet S matrix was constructed and used to calculate transmission probabilities as well as the Wigner delay times.

Transmission resonances result from the interaction of electrons with the oscillating field. A static bound state can serve as an electron reservoir when an oscillating field is applied and electrons can drop there from the propagating channels by photon emission. Similarly, electrons in the static bound state can also absorb photons and feed back into

TABLE I. Comparison of the Wigner delay times and the lifetimes derived from transmission poles.

Resonance	τ_W (sec) [a]	τ_L (sec) [b]
Figure 11	6.4×10^{-10}	1.6×10^{-10}
Figure 12, A	4.3×10^{-7}	1.1×10^{-7}
B	8.4×10^{-14}	3.7×10^{-13}
C	2.9×10^{-8}	7.4×10^{-9}
D	7.8×10^{-9}	1.9×10^{-9}

[a] τ_W: the Wigner delay time derived from the S matrix.
[b] τ_L: the lifetime obtained from the transmission pole.

the propagating channels. The location in energy of the resonance is then governed by the energy of the static bound state. This suggests a potential technique for detecting material geometric structures by measuring Floquet resonant transmissions. It is also shown that the bound state will have a slight ac Stark energy shift under the oscillating field.

Even in the absence of a static bound state, a strong oscillating field localized in space can create the Floquet quasibound states. The energies of these quasibound states can be obtained by locating the singularities of the state matrix or poles of the Floquet S matrix. Floquet quasibound states appear as transmission poles which line up in the complex energy plane with the Floquet energy spacing along the real energy axis of $\hbar\omega$. Lifetimes derived from the transmission poles have the same order of magnitude as the corresponding Wigner delay times.

ACKNOWLEDGMENTS

The authors wish to thank the Welch Foundation Grant No. F-1051, NSF Grant No. INT-9602971, and DOE Contract No. DE-FG03-94ER14405 for partial support of this work. We also thank NPACI and the University of Texas at Austin High Performance Computing Center for use of their computer facilities. We thank K. Na and G. Akguc for helpful discussions. Author Li thanks Hou Yunzhen for programming assistance.

APPENDIX: DERIVATION OF THE FLOQUET S MATRIX

In this Appendix we show how to construct the Floquet S matrix using matrix format. Let us first introduce some relevant matrices whose matrix elements are defined in the following way:

$$(\mathbf{M}_s^{\pm})_{nm}=[(k_n+q_m)e^{-iq_mL/2}\pm(k_n-q_m)e^{iq_mL/2}]J_{n-m}\left(\frac{V_1}{\hbar\omega}\right), \tag{A1}$$

$$(\mathbf{M}_r)_{nm}=2\,k_n\,e^{-ik_nL/2}\delta_{n,m}, \tag{A2}$$

$$(\mathbf{M}_c^{\pm})_{nm}=e^{-i(k_n\pm q_m)L/2}J_{n-m}\left(\frac{V_1}{\hbar\omega}\right), \tag{A3}$$

$$(\mathbf{M}_i)_{nm}=e^{-ik_nL}\delta_{n,m}. \tag{A4}$$

Equation (19) can then be written as

$$\mathbf{M}_s^{\pm}\cdot\mathbf{C}^{\pm}=\mathbf{M}_r\cdot(\mathbf{A}^i\pm\mathbf{B}^i). \tag{A5}$$

When the state matrix $\mathbf{M}_s^{\pm}$ is not singular (Sec. IV discusses the meaning of $\mathbf{M}_s^{\pm}$ when it *is* singular), we can take the inverse of $\mathbf{M}_s^{\pm}$, and the coefficient vector $\mathbf{C}^{\pm}$ becomes

$$\mathbf{C}^{\pm}=(\mathbf{M}_s^{\pm})^{-1}\cdot\mathbf{M}_r\cdot(\mathbf{A}^i\pm\mathbf{B}^i). \tag{A6}$$

The Floquet sideband coefficient vectors are given by

$$\begin{aligned}\mathbf{a}&=\tfrac{1}{2}(\mathbf{C}^{+}+\mathbf{C}^{-})=\tfrac{1}{2}[(\mathbf{M}_s^{+})^{-1}\cdot\mathbf{M}_r\cdot(\mathbf{A}^i+\mathbf{B}^i)\\&\quad+(\mathbf{M}_s^{-})^{-1}\cdot\mathbf{M}_r\cdot(\mathbf{A}^i-\mathbf{B}^i)]\\&=\left[\frac{(\mathbf{M}_s^{+})^{-1}+(\mathbf{M}_s^{-})^{-1}}{2}\right]\cdot\mathbf{M}_r\cdot\mathbf{A}^i\\&\quad+\left[\frac{(\mathbf{M}_s^{+})^{-1}-(\mathbf{M}_s^{-})^{-1}}{2}\right]\cdot\mathbf{M}_r\cdot\mathbf{B}^i\end{aligned} \tag{A7}$$

and

$$\begin{aligned}\mathbf{b}&=\tfrac{1}{2}(\mathbf{C}^{+}-\mathbf{C}^{-})=\left[\frac{(\mathbf{M}_s^{+})^{-1}-(\mathbf{M}_s^{-})^{-1}}{2}\right]\cdot\mathbf{M}_r\cdot\mathbf{A}^i\\&\quad+\left[\frac{(\mathbf{M}_s^{+})^{-1}+(\mathbf{M}_s^{-})^{-1}}{2}\right]\cdot\mathbf{M}_r\cdot\mathbf{B}^i.\end{aligned} \tag{A8}$$

Now rewrite Eqs. (20) and (21) in matrix form,

$$\begin{aligned}\mathbf{A}^o&=\mathbf{M}_c^{+}\cdot\mathbf{a}+\mathbf{M}_c^{-}\cdot\mathbf{b}-\mathbf{M}_i\cdot\mathbf{A}^i\\&=(\tfrac{1}{2}\{\mathbf{M}_c^{+}\cdot[(\mathbf{M}_s^{+})^{-1}+(\mathbf{M}_s^{-})^{-1}]\\&\quad+\mathbf{M}_c^{-}\cdot[(\mathbf{M}_s^{+})^{-1}-(\mathbf{M}_s^{-})^{-1}]\}\cdot\mathbf{M}_r-\mathbf{M}_i)\cdot\mathbf{A}^i\\&\quad+(\tfrac{1}{2}\{\mathbf{M}_c^{+}\cdot[(\mathbf{M}_s^{+})^{-1}-(\mathbf{M}_s^{-})^{-1}]\\&\quad+\mathbf{M}_c^{-}\cdot[(\mathbf{M}_s^{+})^{-1}+(\mathbf{M}_s^{-})^{-1}]\}\cdot\mathbf{M}_r)\cdot\mathbf{B}^i\\&\equiv\mathbf{M}_{AA}\cdot\mathbf{A}^i+\mathbf{M}_{AB}\cdot\mathbf{B}^i\end{aligned} \tag{A9}$$

and

$$\begin{aligned}\mathbf{B}^o&=\mathbf{M}_c^{-}\cdot\mathbf{a}+\mathbf{M}_c^{+}\cdot\mathbf{b}-\mathbf{M}_i\cdot\mathbf{B}^i\\&=(\tfrac{1}{2}\{\mathbf{M}_c^{-}\cdot[(\mathbf{M}_s^{+})^{-1}+(\mathbf{M}_s^{-})^{-1}]\\&\quad+\mathbf{M}_c^{+}\cdot[(\mathbf{M}_s^{+})^{-1}-(\mathbf{M}_s^{-})^{-1}]\}\cdot\mathbf{M}_r)\cdot\mathbf{A}^i\\&\quad+(\tfrac{1}{2}\{\mathbf{M}_c^{-}\cdot[(\mathbf{M}_s^{+})^{-1}-(\mathbf{M}_s^{-})^{-1}]+\mathbf{M}_c^{+}\cdot[(\mathbf{M}_s^{+})^{-1}\\&\quad+(\mathbf{M}_s^{-})^{-1}]\}\cdot\mathbf{M}_r-\mathbf{M}_i)\cdot\mathbf{B}^i\\&\equiv\mathbf{M}_{BA}\cdot\mathbf{A}^i+\mathbf{M}_{BB}\cdot\mathbf{B}^i.\end{aligned} \tag{A10}$$

If we combine Eqs. (A9) and (A10), we obtain

$$\begin{pmatrix}\mathbf{A}^o\\\mathbf{B}^o\end{pmatrix}=\begin{pmatrix}\mathbf{M}_{AA}&\mathbf{M}_{AB}\\\mathbf{M}_{BA}&\mathbf{M}_{BB}\end{pmatrix}\begin{pmatrix}\mathbf{A}^i\\\mathbf{B}^i\end{pmatrix} \tag{A11}$$

$$\equiv\mathcal{S}\begin{pmatrix}\mathbf{A}^i\\\mathbf{B}^i\end{pmatrix}. \tag{A12}$$

Each element $\mathcal{S}_{nm}$ of matrix $\mathcal{S}$ gives the probability amplitude that the electron is scattered from Floquet sideband m to sideband n $[n,m\in(-\infty,\infty)]$. If we keep only the propagating modes $[n,m\in[0,\infty)]$, we then extract the S matrix $\overline{\mathbf{S}}$ from the matrix $\mathcal{S}$ as discussed in Sec. II:

$$\begin{pmatrix}\overline{\mathbf{A}}^o\\\overline{\mathbf{B}}^o\end{pmatrix}=\overline{\mathbf{S}}\begin{pmatrix}\overline{\mathbf{A}}^i\\\overline{\mathbf{B}}^i\end{pmatrix}. \tag{A13}$$

[1] M. Büttiker and R. Landauer, Phys. Rev. Lett. **49**, 1739 (1982); Phys. Scr. **32**, 429 (1985).
[2] J. A. Stovneng and E. H. Hauge, J. Stat. Phys. **57**, 841 (1989).
[3] M. Wagner, Phys. Rev. B **49**, 16 544 (1994); Phys. Rev. A **51**, 798 (1995); Phys. Rev. Lett. **76**, 4010 (1996); Phys. Status Solidi B **204**, 382 (1997); Phys. Rev. B **55**, R10 217 (1997); **57**, 11 899 (1998).
[4] D. S. Saraga and M. Sassoli de Bianchi, Helv. Phys. Acta **70**, 751 (1997).
[5] Q. Sun, J. Wang, and T. Lin, Phys. Rev. B **58**, 13 007 (1998).
[6] G. Burmeister and K. Maschke, Phys. Rev. B **57**, 13 050 (1998).
[7] G. Burmeister and K. Maschke, Phys. Rev. B **59**, 4612 (1999).
[8] G. A. Luna-Acosta, G. Orellana-Rivadeneyra, A. Mendoza, and C. Jung, Chaos Solitons Fractals (to be published).
[9] R. Tsu and L. Esaki, Appl. Phys. Lett. **22**, 562 (1973).
[10] L. P. Kouwenhoven, S. Jauhar, J. Orenstein, P. L. McEuen, Y. Nagamune, J. Motohisa, and H. Sakaki, Phys. Rev. Lett. **73**, 3443 (1994).
[11] R. H. Blick, R. J. Haug, D. W. van der Weide, K. von Klitzing, and K. Eberl, Appl. Phys. Lett. **67**, 3924 (1995).
[12] H. Drexler, J. S. Scott, S. J. Allen, K. L. Campman, and A. C. Gossard, Appl. Phys. Lett. **67**, 2816 (1995).
[13] B. J. Keay, S. J. Allen, Jr., J. Galán, J. P. Kaminski, K. L. Campman, A. C. Gossard, U. Bhattacharya, and M. J. W. Rodwell, Phys. Rev. Lett. **75**, 4098 (1995); B. J. Keay, S. Zeuner, S. J. Allen, Jr., K. D. Maranowski, A. C. Gossard, U. Bhattacharya, and M. J. W. Rodwell, *ibid.* **75**, 4102 (1995).
[14] G. S. Vieira, S. J. Allen, P. S. S. Guimarães, K. L. Campman, and A. C. Gossard, Phys. Rev. B **58**, 7136 (1998).
[15] J. H. Shirley, Phys. Rev. **138**, B979 (1965).
[16] M. Holthaus and D. Hone, Phys. Rev. B **47**, 6499 (1993).
[17] T. Fromherz, Phys. Rev. B **56**, 4772 (1997).
[18] A. K. Kazanskii, V. N. Ostrovskii, and E. A. Solovev, Zh. Éksp. Teor. Fiz. **70**, 493 (1976) [Sov. Phys. JETP **43**, 254 (1976)].
[19] P. F. Bagwell and R. K. Lake, Phys. Rev. B **46**, 15 329 (1992).
[20] G. P. Berman, E. N. Bulgakov, D. K. Campbell, and A. F. Sadreev, Physica B **225**, 1 (1996); E. N. Bulgakov and A. F. Sadreev, J. Phys.: Condens. Matter **8**, 8869 (1996).
[21] P. K. Tien and J. P. Gordon, Phys. Rev. **129**, 647 (1963).
[22] M. Büttiker, Phys. Rev. Lett. **57**, 1761 (1986); R. Landauer, J. Phys.: Condens. Matter **1**, 8099 (1989).
[23] U. Fano, Phys. Rev. **124**, 1866 (1961); E. Tekman and P. F. Bagwell, Phys. Rev. B **48**, 2553 (1993).
[24] L. D. Landau and E. M. Lifshitz, *Quantum Mechanics* (Pergamon Press, Oxford, 1976), p. 555; G. Baym, *Lectures on Quantum Mechanics* (W. A. Benjamin, Inc., Massachusetts, 1973), p. 108.
[25] K. Na and L. E. Reichl, Phys. Rev. B **59**, 13 073 (1999).